the system and ram air balloon inflation is accomplished through the one-way scoops located circumferentially on the balloon envelope near the balloon equator. A three-dimensional Y-bridle assembly attached to the inside of the balloon at the equator mechanically intiates the flare ignition sequence when the balloon has reached about 90% inflation (Fig. 3-5). This technique of environmental sensing and arming eliminates the need for a safe position on the mechanical timer.

The heat generator, a molded phenolicasbestos case containing a propellant composition, is housed in the interface hardware ahead of the flare candle and is in line with the lower throat of the balloon. The propellant grain is tailored to burn at a rate sufficient to provide a large volume of hot gas to induce the required thermal buoyancy into the balloon. Upon ignition the flare ignitor directs an intense short duration flame on the heat generator and flare candle; thus, both compositions are ignited at the same time. The heat generator output is directed into the balloon, thereby heating and lowering the density of the air in the balloon. The burning flare melts an aluminum separation ring, thus allowing the candle to separate from the interface hardware. As the candle falls the suspension cables, which are joined to a single cable fastened to and stored on the base of the candle, cause the candle to tip over burning face down and arrest the candle 20 ft below the balloon (Fig. 3-6). As the buoyancy increases in the balloon, the downward trajectory is slowed to a mean rate of 5 fps (Fig. 4). This descent rate is maintained by the residual heat in the balloon and the burning flare candle. Although a true hover-type trajectory could be accomplished, a slight downward rate is desirable to keep the dense smoke that is emitted by the burning candle from obscuring the light output.

As the candle burns, its weight loss tends to be compensated for by the loss of heat from the balloon. However, the decrease in weight is greater than the decrease in buoyancy. To compensate for this nonlinear weight-buoyancy phenomenon, a vent is cut in the balloon top 260 sec after drogue chute deployment. The vent increases the balloon heat loss and the mean descent rate of 5 fps is maintained. Some 320 sec after drogue chute deployment the self-destruct system cuts a large opening in the balloon, thus releasing the entrapped hot air. The rapid deflation causes the system to descend to the ground at approximately 20 fps, thereby clearing the airspace of the spent system.

The hot air buoyancy/deceleration design configuration as shown in Fig. 3-6 is a natural shaped hot-air balloon with a maximum inflation diameter of 20 ft. It is packed at a density of 40 lb/ft^3 in a heavy cotton duck deployment bag. A natural-shaped balloon is practically free of circumferential stresses. Almost all the suspended load stresses are meridional. The envelope is constructed of gores sewn together according to basic parachute fabrication techniques. Ram-air-inflation scoops are located near the balloon equator. The lower gores extend on the under side of the upper gores and bear against the lower portion of the upper gore to provide a positive seal when the balloon is fully inflated. Upper gore material is 1.55-oz nylon and lower gore material is 1.30 oz. A calendered and catonic coating process reduces the permeability and enchances the high-density packing properties of the nylon fabric.

Operational conditions of the balloon are in a Reynolds number range of 10^5 to 10^6 and a burble fence is required to prevent coning action of the balloon. A flying fence design was derived to provide uniform flow separation and permit easy packing of the balloon at high density.

The Briteye Flare program has resulted in an advanced design flare system with a light output of 5 million candlepower, burn duration of 5 min, slow terminal descent, and the capability of being carried on external wing racks of high-speed aircraft. Of primary importance in the field of aerodynamic deceleration is the development of a midair-deployed, ram-air-inflated, hot-air buoyancy balloon suspension system. The development of this system has advanced the technology of this type of decelerator/buoyancy aerostat to the point at which computer derived mathematical models of the flight trajectory can be correlated with actual flights. With this understanding this technology can be and is being applied to other applications.

Gust Design Envelope of Interacting Loads

KENNETH L. ROGER*
The Boeing Company, Wichita, Kansas

Introduction

WHEN airframe stress is a function of n loads, the critical loading combinations form an n-dimensional surface bordering the design loading region. When the surface is known, techniques are available for computing whether or not the stress will satisfy a random-gust design requirement.[1]

This Note presents an alternate approach wherein the design requirement and the gust load covariances are used to directly define the boundaries of the gust-loading region. This approach is particularly useful to the loads engineer who must specify gust design load envelopes independent of the stress-to-load relationship.

Points on the boundaries of the gust-loading region are defined by a parametric inequality involving the n loads. The design envelope is found by eliminating the parameters. An especially simple analytic solution is found for the design load envelope satisfying the U_σ gust criteria.[2]

Mathematical Definition of the Design Load Envelope

If x, consisting of x_{mean} plus Δx, is the general linear combination of n loads L_i, then, using matrix notation,

$$\Delta x = \{C_i\}^T \{\Delta L_i\} \tag{1}$$

The variances of x and $\dot{x}$ are related to the covariances of $\{\Delta L_i\}$ and $\{\dot{L}_i\}$ (for random-gust inputs) as

$$\sigma_x^2 = \{C_i\}^T [\sigma_{L_{ii}}^2] \{C_i\} \tag{2}$$

and

$$\sigma_{\dot{x}}^2 = \{C_i\}^T [\sigma_{\dot{L}_{ii}}^2] \{C_i\} \tag{3}$$

The design region of ΔL, ΔL_2, ..., ΔL_n includes all points which, for all possible combinations of C_1, C_2, ..., C_n, satisfy the design criteria inequality. For example, Eqs. (4) and (5) represent the U_σ design gust and an exceedance criteria, respectively, where U_σ and N are specified in the criteria;

$$F_{U\sigma}(\Delta x, \sigma_x) = (\Delta x)^2 - U_\sigma^2 \sigma_x^2 \leq 0 \tag{4}$$

$$F_{\text{exc}}(\Delta x, \sigma_x, \sigma_{\dot{x}}) = (\text{exceedances of } \Delta x) - N \leq 0 \tag{5}$$

Using Eqs. (1–3), the selected design inequality can be written in terms of ΔL_1, ΔL_2, ..., ΔL_n and the parameters C_1, C_2, ..., C_n.

The design loads envelope is the boundary of the gust-loading region. It includes all of the potentially critical

Received March 19, 1969.

* Structures Engineer, Wichita Division. Member AIAA.

loading combinations which must be investigated by the stress analyst. The envelope is found by eliminating the parameters using any n of the following $n + 1$ equations:

$$\begin{aligned} F(L_1, \ldots, L_n; C_1, \ldots, C_n) &= 0 \\ \partial F/\partial C_1 &= 0 \\ &\cdot \\ &\cdot \\ &\cdot \\ \partial F/\partial C_n &= 0 \end{aligned} \tag{6}$$

Using an exceedance criteria, such as Eq. (5), points on the envelope can be found using numerical approximations of the partial derivatives, then solving simultaneous algebraic equations. The author has used this technique for $n = 2$ and $n = 3$.

Design Load Envelopes for the U_σ Criteria

Using the U_σ design criteria of Eq. (4), and using Eqs. (1) and (2), the parametric equation of the design surface becomes

$$F_{U\sigma}(\Delta L_i, C_i) = (\{C_i\}^T\{\Delta L_i\})^2 - U_\sigma^2\{C_i\}^T[\sigma_{L_{ij}}^2]\{C_i\} = 0$$

which can be written as

$$F_{U\sigma}(\Delta L_i, C_i) = \{C_i\}^T(\{\Delta L_i\}\{\Delta L_i\}^T - U_\sigma^2[\sigma_{L_{ij}}^2])\{C_i\} = 0 \tag{7}$$

so that

$$\left\{\frac{\partial F}{\partial C_i}\right\} = 2(\{\Delta L_i\}\{\Delta L_i\}^T - U_\sigma^2[\sigma_{L_{ij}}^2])\{C_i\} = 0 \tag{8}$$

Substituting,

$$\begin{aligned} \{\bar{C}_i\} &= [Z]\{C_i\} \\ \{\alpha_i\} &= [Z]^{-1}\{\Delta L_i\} \end{aligned} \tag{9}$$

where

$$[Z] = U_\sigma[\sigma_{L_{ij}}^2]^{1/2}$$

($[Z]$ will be real; any of the symmetric square roots may be used.) Equation (8) becomes

$$(\{\alpha_i\}\{\alpha_i\}^T - [I])\{\bar{C}_i\} = 0 \tag{10}$$

Recalling that a matrix formed as the outer product of a vector has only one nonzero eigenvalue, it is seen that Eq. (9) is satisfied if and only if the trace of $\{\alpha_i\}\{\alpha_i\}^T$ equals unity.

Thus, Eq. (9) plus the solution of Eq. (10) give the general solution for design load envelopes satisfying the U_σ criteria.

All points on the design limit surface are given by

$$\{L_i\} = \{L_{\text{mean}_i}\} + U_\sigma[\sigma_{L_{ij}}^2]^{1/2}\{\alpha_i\} \tag{11a}$$

where $\{\alpha_i\}$ are points on the unit n-dimensional sphere

$$\alpha_1^2 + \alpha_2^2 + \ldots + \alpha_n^2 = 1 \tag{11b}$$

and where $[\sigma_{L_{ij}}^2]^{1/2}$ is any of the symmetric square roots of the load covariance matrix. The required matrix square root can be found using standard modal analysis methods.

References

[1] Houbolt, J. C., "Exceedances of Structural Interaction Boundaries for Random Excitation," AFOSR 68-0032, Dec. 1967, Air Force Office of Scientific Research, Arlington, Va.

[2] Hoblit, F. M. et al., "Development of a Power-Spectral Gust Design Procedure for Civil Aircraft," ADS-53, Jan. 1966, Federal Aviation Agency.

Distribution of Lengths of High-Altitude Clear Air Turbulent Regions

EDWARD V. ASHBURN*
Lockheed-California Company, Burbank, Calif.

CROOKS et al.[1] used the results of the analysis of high-altitude clear air turbulence (HICAT) flights 39–175 to determine some measures of the size of HICAT regions. The analysis of the latest series of HICAT flights (flights 180–285) have now been published.[2] In this Note, these new data have been combined with the older data to provide the basis for a determination of the distribution of lengths of HICAT regions. The results of this work are displayed in Fig. 1.

A total of 704 samples for which the flight path was level and the turbulence was indicated to be greater than very light were used to determine the distribution of lengths of the turbulent regions. The percentages of exceedances are given for the total sample, for cases of moderate or greater turbulence (144 cases), for severe turbulence (16 cases), and for those cases for which power spectra and time histories were computed. Time histories and power spectra were computed for only those cases where there was no obvious malfunction of the instruments and the length of the sample was adequate for a power spectra analysis.

The usefulness and the interpretation of the results presented in Fig. 1 depend, to a significant degree, upon the definitions of a turbulent region that were used in preparing the Test Summary Tables of Refs. 1 and 2. The definitions given by Crooks[1] are paraphrased as follows. The selection of clear air turbulence samples was based upon an edit of the flight measurements recorded upon a "quick-look" oscillogram. Turbulence samples were selected primarily from an evaluation of the c.g. normal acceleration response of the aircraft. If continuous rapid c.g. acceleration disturbances in excess of $\pm 0.05\ g$ were observed, turbulence was considered to be present. A turbulent region thus defined was considered to be significant (i.e., the data worth processing) if frequent c.g. acceleration peaks of $\pm 0.10\ g$ or more were observed. In this event, sample (called run and given a number) start and stop times were noted to the nearest 5 sec. Samples of less than 10-sec duration were ignored. Each edited sample was also placed into one of the following categories as shown in Table 1. These criteria were used for sample selection only. The correlation between these criteria and computed gust velocity is good but not perfect.

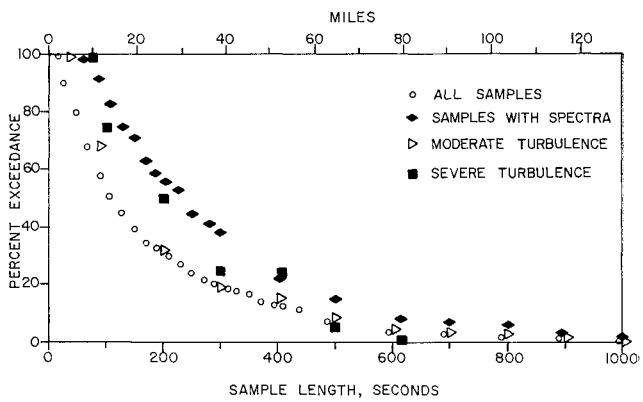

Fig. 1 Percent exceedances of horizontal lengths of high-altitude clear air turbulent regions.

Received May 5, 1969. This work supported under Air Force Flight Dynamics Laboratory, Wright-Patterson Air Force Base, Ohio, under Contract AF-F33615-69-C-1033.

* Head, Atmospheric Physics Laboratory, Rye Canyon Research Center. Member AIAA.